NASA Technical Memorandum 107471

Strong, Tough, and Pest Resistant $MoSi_2$-Base Hybrid Composite for Structural Applications

M.G. Hebsur
NYMA, Inc.
Brook Park, Ohio

and

M.V. Nathal
Lewis Research Center
Cleveland, Ohio

Prepared for the
Second International Symposium on Structural Intermetallics
sponsored by The Minerals, Metals, and Materials Society
Seven Springs, Pennsylvania, September 21–26, 1997

National Aeronautics and
Space Administration

STRONG, TOUGH, AND PEST RESISTANT $MoSi_2$-BASE HYBRID COMPOSITE FOR STRUCTURAL APPLICATIONS

M. G. Hebsur
NYMA, Inc.
Brook Park, OH 44142

and

M. V. Nathal
NASA Lewis Research Center
Cleveland, OH 44135

Abstract

Addition of about 30 to 50 vol % of Si_3N_4 particulate to $MoSi_2$ improved resistance to low temperature accelerated oxidation by forming a Si_2ON_2 protective scale and thereby eliminating catastrophic 'pest failure'. The Si_3N_4 addition also improved the high temperature creep strength by nearly five orders of magnitude, doubled the room temperature toughness and significantly lowered the CTE of the $MoSi_2$ and eliminated matrix cracking in SCS-6 reinforced composites even after thermal cycling. The SCS-6 fiber reinforcement improved the room temperature fracture toughness by seven times and impact resistance by five times. The composite exhibited excellent strength and toughness improvement up to 1400 °C. More recently, tape casting was adopted as the preferred processing of $MoSi_2$-base composites for improved fiber spacing, ability to use small diameter fibers, and for lower cost. Good strength and toughness values were also obtained with fine diameter Hi-Nicalon tow fibers. This hybrid composite remains competitive with ceramic matrix composites as a replacement for Ni-base superalloys in aircraft engine applications.

Introduction

Advanced high temperature materials are key to successfully developing the next generation aerospace propulsion and power systems (1). Advanced materials will enhance the performance of these systems by allowing higher speeds, expanded flight ranges, and increased payload capabilities. Due to high specific strength and stiffness, and the potential for increased temperature capability, composite materials are attractive for systems ranging from subsonic commercial aircraft to future space propulsion and power systems. Based on high temperature oxidation behavior, it appears that $MoSi_2$ is one of the few intermetallics to have potential for further development. Since $MoSi_2$ is a silica former, it can withstand at least 200 °C higher temperatures (up to 1500 °C) than alumina formers such as NiAl (2). It also has a higher melting point (2023 °C) and lower density (6.2 gm/cc) than superalloys, and has electrical and thermal conductivity advantages over ceramics (3).

However, the use of $MoSi_2$ has been hindered due to the brittle nature of the material at low temperatures, inadequate creep resistance at high temperatures, accelerated ('pest') oxidation at temperatures between approximately 400 and 500 °C, and its relatively high coefficient of thermal expansion (CTE) compared to potential reinforcing fibers such as SiC. The CTE mismatch between the fiber and the matrix results in severe matrix cracking during thermal cycling.

In the last 12 years, an extensive amount of work has been carried out in efforts to improve the high temperature properties of $MoSi_2$ by solid solution alloying, discontinuous reinforcement, and fiber reinforcement. Alloying with W (4) or Re (5) has improved high temperature creep strength. Substantial improvements in strength have also been achieved by adding particulates, platelets or whiskers of SiC (6), TiB_2, and HfB_2 (7). However, the effects of grain refinement may limit the creep strength of these types of composites (8). To date, $MoSi_2$ alloyed with W and containing 40 vol % SiC has achieved the creep strength superior to that of the superalloys, although not the best monolithic ceramics. The addition of SiC whiskers has also yielded improvements in room temperature toughness (9). However, it appears that the strength and damage tolerance required for high temperature aerospace applications can only be achieved by reinforcement with high strength continuous fibers.

Nb fibers (10) have been shown to improve the strength and toughness but this option is limited by a severe reaction between the Nb fiber and $MoSi_2$. Maloney and Hecht (11) have done extensive work on the development of continuous fiber reinforced $MoSi_2$ base composites to achieve high temperature creep resistance and room temperature toughness. Candidate fibers consisted of fibers, such as SiC, single crystal Al_2O_3, ductile Mo, and W alloy fibers. The refractory metal fibers increased both creep strength and fracture toughness, although reaction with the matrix was still a problem. The addition of about 40 vol % of SiC in the form of whiskers and particulate was used to lower the thermal expansion of the $MoSi_2$ base matrix and prevented matrix cracking in these composites. However, matrix cracking was still observed in an SCS-6 fiber reinforced composite even with the matrix containing up to 40 vol % SiC whiskers. This composite also suffered catastrophic pest attack at 500 °C. Sapphire fiber reinforced composites showed no evidence of matrix cracking due to the good thermal expansion match between $MoSi_2$ and Al_2O_3. However, the strong fiber-matrix bond did not provide any toughness improvement.

$MoSi_2$ has been known to be susceptible to pesting, which is usually defined as disintegration into powder, and appears to be most pronounced near 500 °C (12-14). The pesting phenomenon in $MoSi_2$ is considered to result from accelerated oxidation, which involves the simultaneous formation of MoO_3 and SiO_2 in amounts

essentially determined by the Mo and Si concentrations in the intermetallic. The accelerated oxidation is a necessary but not sufficient condition for pesting. In some but not all cases, pesting has been linked to the formation of voluminous Mo oxides in porosity or microcracks. Improvements in fabrication of $MoSi_2$ have led to materials which had less porosity and were less susceptible to pest attack. Because of increased surface areas and complexities of fabrication from incorporating reinforcement phases in $MoSi_2$ based composites, pesting of composite materials is still a major concern (11,13). Microalloying with Ge (15) and macroalloying with Cr (16) have also been shown to improve pesting resistance.

In earlier work (17) of developing $MoSi_2$ suitable for SiC fiber reinforcement, it was found that the addition of about 30 to 50 vol % of Si_3N_4 particulate to $MoSi_2$ improved the low temperature accelerated oxidation resistance by forming a Si_2ON_2 protective scale and thereby eliminated catastrophic pest failure. The Si_3N_4 addition also improved the high temperature oxidation resistance and compressive strength. The brittle-to-ductile (BDTT) transition-temperature of $MoSi_2$-30 vol % Si_3N_4, measured in four-point bending, was between 900 and 1000 °C. More importantly, the Si_3N_4 addition significantly lowered the CTE of the $MoSi_2$ and eliminated matrix cracking in SCS-6 reinforced composites even after thermal cycling (14,18).

These encouraging preliminary results led to a joint program for further development between Pratt & Whitney, the Office of Naval Research, and NASA Lewis. The overall technical direction of this long range program is to develop these composite system for advanced aircraft engine application as a competitor to both today's superalloys and other advanced materials, primarily ceramic matrix composites. A turbine blade outer air seal for Pratt & Whitney's ATEGG/JTD engine demonstrator was chosen as the first component upon which to focus. This paper briefly describes the progress made so far in developing, processing, and characterizing $MoSi_2$ base hybrid composites.

Materials and Procedures

Attrition milling of $MoSi_2$ and Si_3N_4 powder is the first step in composite processing. Several batches containing a mixture of commercially available $MoSi_2$ and either 30 or 50 vol % of Si_3N_4 were mechanically alloyed in a Union Process attritor. No densification aids were added to the $MoSi_2$-Si_3N_4 mixtures. The average mean particle size of the mixture after milling was 1.25±0.71 μm at 99 % confidence. The $MoSi_2$-Si_3N_4 powder was consolidated into "matrix-only" plates 12 cm long x 5 cm wide x 0.3 cm thick, or a larger size of 18 cm long x 2.5 cm wide x 1.25 cm thick. The plates were consolidated by vacuum hot pressing followed by hot isostatic pressing to achieve full density. Further consolidation of the hot pressed plate was achieved by hot isostatic pressing (HIP). Composite plates of various thickness consisting of 6, 12, or 56 plies of 30 vol % SCS-6 fibers having 0, 0/90 and 90 orientations in the $MoSi_2$-Si_3N_4 matrix were prepared by the powder cloth technique (15) and consolidated in the same manner as the material without fibers. The two-step consolidation process enabled the use of a lower consolidation temperature than could be used if hot pressing was used alone. This resulted in a fully dense material without excessive reaction or damage to the fibers.

From the consolidated material, ASTM standard specimens for several tests such as compression, fracture toughness, impact and oxidation were machined by electro discharge machining (EDM) and grinding techniques. Tensile tests were conducted on 1.27 by 15 cm straight or dog bone-shaped specimens machined from 6 ply composite panels. Tests were performed in air between 25 and 1200 °C at constant strain rate of 1.4×10^{-3} cm sec^{-1}. Constant load compression creep tests were conducted on $MoSi_2$-50Si_3N_4 specimens at 1200 °C in the stress range of 40 to 400 MPa in air. Fracture toughness tests were measured on chevron notched bend specimens made from 12 ply composite panels, tested at a constant strain rate of 1.2×10^{-5} cm/min. ASTM full size Charpy V-notch impact specimens were machined from 56 ply composites and impact tests were conducted using 356 J Tinus Olsen impact tester with Dynatrup instrumentation. The heating of the specimen was carried out using two oxypropane torches. The temperature was monitored using a laser pyrometer. Tensile creep-rupture tests were performed in vacuum between 1100 to 1200 °C 70 MPa were conducted on hybrid composites using an MTS machine fitted with water cooled grips and a side-contact extensometer. Oxidation coupons typically were 1.2 x 1.2 x 0.25 cm and were ground and polished to final 1 μm diamond polish. In the case of composites, no attempt was made to coat the exposed fibers. Detailed microstructural characterization of as-fabricated and tested specimens were carried out using standard optical and electron microscopic techniques.

Results and Discussion

Microstructure of as-fabricated materials:

Figure 1(a) shows the microstructure of the as-consolidated $MoSi_2$-Si_3N_4 monolithic matrix. The Si_3N_4 particles are interconnected and well dispersed in the $MoSi_2$ matrix. As the volume fraction of Si_3N_4 particulate increased, the degree of interconnectivity of the Si_3N_4 phase increased, although even at 50 vol % nitride, the materials could still be machined by EDM. As expected from thermodynamic predictions, the Si_3N_4 particles appeared to be quite stable, with very little or no reaction with the $MoSi_2$ even after exposure at 1500 °C. X-ray diffraction of $MoSi_2$-Si_3N_4 showed only the presence of $MoSi_2$ (tetragonal) and a mixture of α and β Si_3N_4 phases. Even though there is a significant CTE mismatch between $MoSi_2$ and Si_3N_4, the small particle size prevented thermally induced microcracking. TEM examination, Fig.1(b), performed on $MoSi_2$-Si_3N_4 also confirmed no reaction between $MoSi_2$ and Si_3N_4. In some isolated areas very fine Mo_5Si_3 phase was detected. This is believed to have been present in the as-procured $MoSi_2$ powder. Figure 2 shows the transverse microstructure of the as-fabricated SCS-6/$MoSi_2$ composite. A reaction zone around the fibers was generally less than 1 μm in thickness and resulted from reaction of the carbon layer to form SiC and Mo_5Si_3. Although the fiber distribution is not uniform, Fig. 2 indicates the absence of matrix cracking. The CTE measurements made on the matrix-only plate and composites plotted as a function of temperature are compared with the monolithic constituents in Fig. 3. It is clear from Fig. 3 that the addition of Si_3N_4 to $MoSi_2$ has effectively lowered the CTE of the matrix, achieving the desired result of eliminating matrix cracking. Furthermore, no cracks were found in either the matrix or the reaction zone even after 1000 thermal cycles between 1200 and 200 °C. These results show that the use of Si_3N_4 was much more effective than similar attempts (9) using SiC.

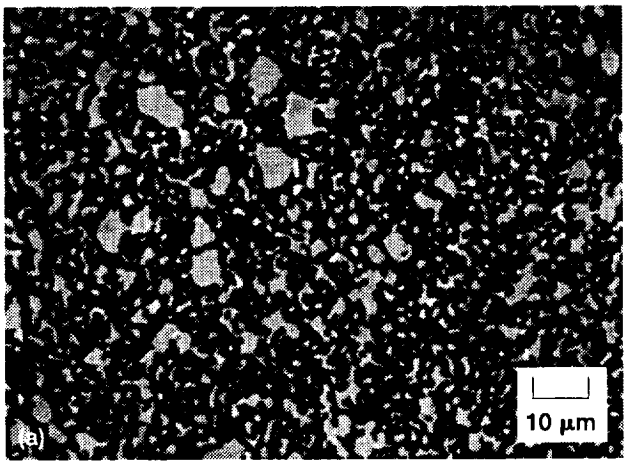

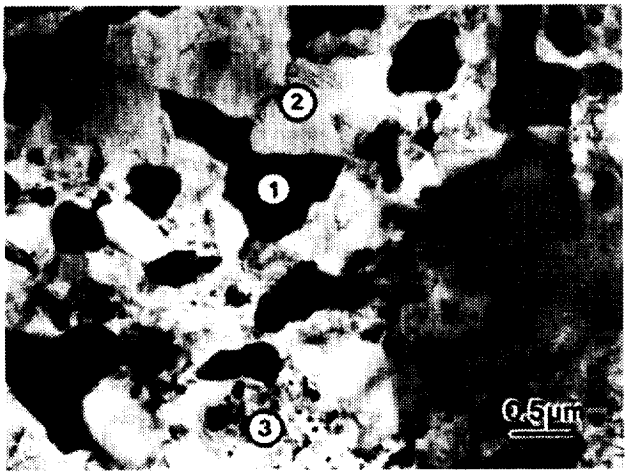

Figure 1.—Micrographs of $MoSi_2$-Si_3N_4 monolithic matrix (a) SEM micrograph of consolidated $MoSi_2$-$50Si_3N_4$ ($MoSi_2$ is the light phase). (b) TEM micrograph of HP + HIP'ed $MoSi_2$-$50Si_3N_4$ showing (1) $MoSi_2$ phase (2) Si_3N_4 phase, and (3) a region containing fine Mo_5Si_3 phase.

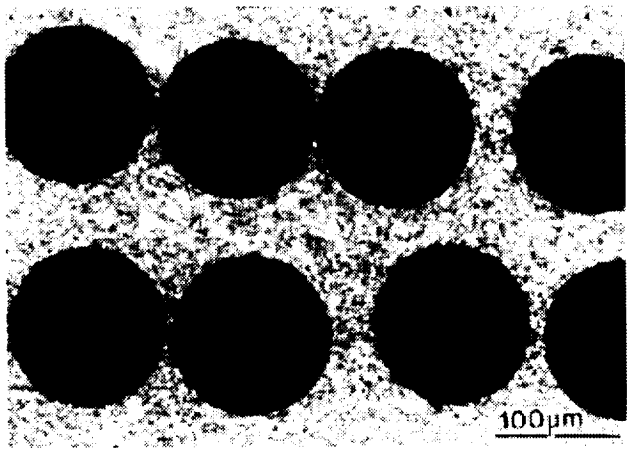

Figure 2.—SEM-BS image of powder cloth fabricated SCS-6/$MoSi_2$-$30Si_3N_4$ hybrid composite.

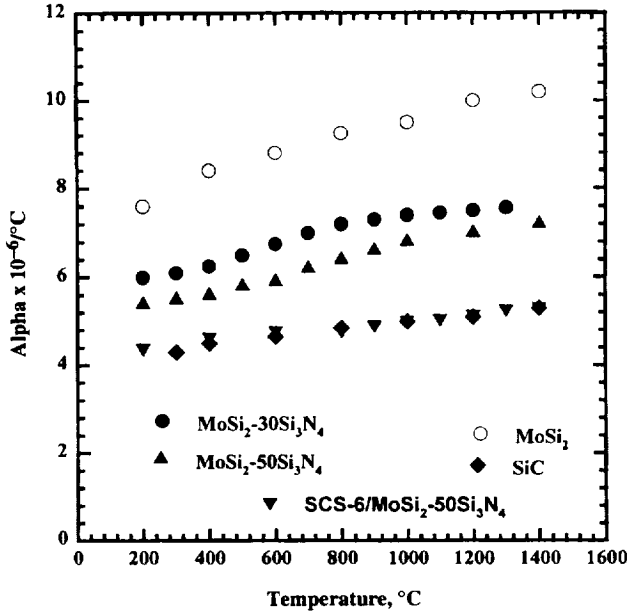

Figure 3.—Thermal expansion data for several $MoSi_2$-base materials and SiC refractory phase.

Oxidation Behavior of $MoSi_2$-Base Composites

Since the low temperature oxidation and pesting phenomenon are limiting factors for structural applications of $MoSi_2$-base composites, several critical tests were designed to examine the pesting response. Initially, cyclic oxidation tests were conducted at 400, 500 and 600 °C for 200 cycles. Each cycle consisted of 55 minutes of heating and 5 minutes of cooling. The weight gain at 500 °C was comparatively higher than at 400 and 600 °C, which again confirms the previous observation (10) that 500 °C is the temperature for maximum accelerated oxidation/pest for $MoSi_2$-base alloys. It was therefore decided that 500 °C would be used for all subsequent experiments to examine the oxidation behavior in more detail.

Figure 4(a) shows the specific weight gain versus number of cycles at 500 °C. Both $MoSi_2$-$30Si_3N_4$ and 50 Si_3N_4 show very little weight gain indicating the absence of accelerated oxidation. X-ray diffraction analysis of both these specimens indicated strong peaks of Si_2ON_2 and the absence of MoO_3. The $MoSi_2$ exhibited accelerated oxidation followed by pesting. Initial studies on TEM oxidized $MoSi_2$ samples indicated that oxide formed on $MoSi_2$ is a two phase lamellar structure (Fig. 4(b)) consisting of MoO_3 and amorphous SiO_2. This kind of lamellar structure could provide an easy diffusion path for oxygen, favoring the formation of the MoO_3. The TEM examination of a $MoSi_2$-30 Si_3N_4 specimens oxidized at 500 °C for 1000 hours, Fig. 4(c), showed an order of magnitude decrease in oxide thickness and a disruption of the lamellar oxide structure. However, fine features of the scale in Fig. 4(c) have not analyzed.

Several critical oxidation tests were carried out at 500 °C to examine the influence of pre-existing cracks and superimposed stresses on $MoSi_2$-30 Si_3N_4 materials. These tests included oxidation of bend bars which were precracked using 250 N load and a Vickers indentor. Both uncracked and precracked specimens were oxidized under unstressed, compressive, or tensile stresses. All these tests were

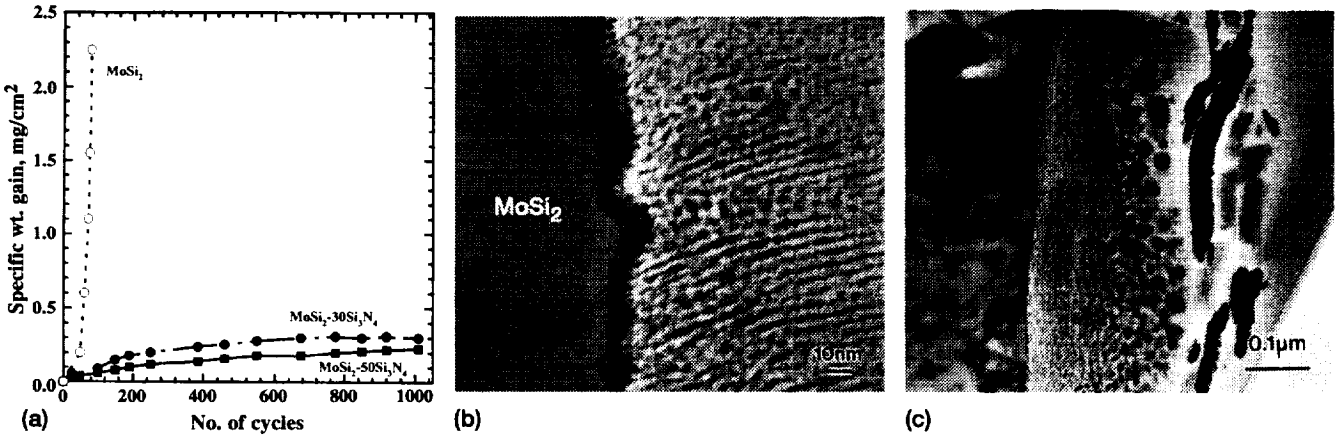

Figure 4.—Oxidation behavior of $MoSi_2$-base materials cyclic oxidized at 500 °C in air. (a) Specific weight versus number of cycles for various $MoSi_2$-base materials. (b) TEM micrograph of $MoSi_2$. (c) TEM micrograph of $MoSi_2$-$30Si_3N_4$ oxidized for 1000 hours.

extended to 1000 hours, with no indications of pesting or premature failure. Finally, burner rig tests were conducted using a jet fuel on two specimens with different degrees of surface roughness, and both specimens came out without showing any evidence of pesting.

Under similar conditions the hybrid composite specimens showed much less weight gain than the matrix-only material. However, the carbon layer on the exposed ends of SCS-6 fibers did oxidize, which influenced the weight gain measurement. Figure 5 shows the SCS-6/$MoSi_2$ and SCS-6/$MoSi_2$-$30Si_3N_4$ composites exposed at 500 °C. The SCS-6/$MoSi_2$ specimen, which had matrix cracks, was completely disintegrated into powder within 24 cycles, whereas the SCS-6/$MoSi_2$-30 Si_3N_4 specimen was intact even after 200 cycles. This is again in strong contrast to previous work (11), where both SCS-6/$MoSi_2$-40 vol % SiC and Al_2O_3/$MoSi_2$ composites were reduced to powder after exposure at 500 °C. All of these observations are consistent with the elimination of pest attack in $MoSi_2$-Si_3N_4 composites due to a mechanism involving elimination of the accelerated oxidation associated with a nonprotective MoO_3 oxide scale. The Si_2ON_2 scale forms rapidly, and is protective even at cracks, pores, and interfaces.

Previous work on high temperature oxidation resistance of this material was restricted to isothermal exposures on the nitride-containing material only. This has now been extended to include cyclic oxidation, on both the matrix and the hybrid composite. The results of cyclic oxidation tests at 1250 °C, which more closely approximates the conditions under which the material would be subjected in a structural application, are shown in Fig. 6. The materials in Fig. 6 were subjected to 1 hour heating cycles to 1250 °C, followed by 20 minutes cooling cycles. It can be seen that the $MoSi_2$-50 Si_3N_4 particulate composite exhibited superior oxidation resistance as compared to $MoSi_2$ alone. The specific weight gain of $MoSi_2$-$50Si_3N_4$ was only about 1 mg/cm^2 in 1000 hours, almost comparable to CVD SiC, which is considered the best SiO_2 former available. The composite initially lost weight due to oxidation of the carbon on the SCS-6 fiber. This was followed by steady weight gain, less than 2 mg/cm^2 in 1000 hours. X-ray diffraction of surface oxides on $MoSi_2$-50 Si_3N_4 and hybrid composites indicated strong peaks of α-cristobalite, which is a crystalline form of SiO_2 and a protective oxide.

Mechanical Properties of $MoSi_2$-Si_3N_4

Previous work (17,18) showed that the nitride additions substantially increased compressive strength at all temperatures. This has been augmented with testing to further characterize this material. Figure 7 shows the results of constant load compression creep tests at 1200 °C on $MoSi_2$-$50Si_3N_4$ plotted as second stage creep rate versus specific stress. For comparison, several materials such as $MoSi_2$, $MoSi_2$-40SiC (8), and a single crystal Ni-base superalloy (20) are also included. $MoSi_2$-$50Si_3N_4$ is almost five orders of magnitude better creep rate than binary $MoSi_2$ and comparable to $MoSi_2$-40SiC. This again confirms the previous observation of beneficial effects of particulate reinforcement. The derived stress exponent, n = 5.3 and the activation energy = 520 kJ/mol calculated from the temperature dependence of creep rate at constant stress, imply a diffusion controlled dislocation mechanism as the rate controlling mechanism.

The fracture toughness of $MoSi_2$ and $MoSi_2$-$30Si_3N_4$ base materials were measured on chevron notched four-point bend specimens, and a finite element/slice model was used to calculate the K_c (21). Figure 8 shows the plot of fracture toughness of $MoSi_2$-Si_3N_4 as a function of temperature. For comparison, two monolithic ceramics SiC and Si_3N_4 are also included in the figure (22). The room temperature fracture toughness of both $MoSi_2$-$30Si_3N_4$ and $50Si_3N_4$ matrix was ~5.2 MPa$\sqrt{m}$, which is about twice the value measured on monolithic $MoSi_2$. Figure 8 also shows that fracture toughness of $MoSi_2$-Si_3N_4 increases with temperature, especially beyond 1000 °C, which is the BDTT for this material. The ceramics chosen for comparison were made by hot pressing techniques that are similar to those used to make $MoSi_2$. In situ toughened Si_3N_4 (23) exhibits higher toughness values, approaching 10 MPa$\sqrt{m}$. But, all of the ceramics maintain the same toughness as temperature is increased.

Mechanical Properties of SCS-6/$MoSi_2$-Si_3N_4 Composites

Figure 9 shows the load verses displacement plot for SCS-6/$MoSi_2$-$30Si_3N_4$ monolithic chevron notched four-point bend specimens tested at room temperature. The composite specimen did not break even after testing for two hours. The apparent critical stress intensity factor, K_Q, calculated from the maximum load data was greater than 35 MPa$\sqrt{m}$ indicated that the hybrid composite specimen was seven

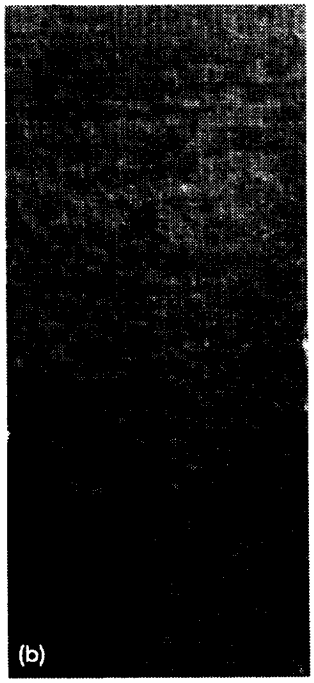

Figure 5.—SCS-6 fiber-reinforced specimens cyclic oxidized at 500 °C in air. (a) $MoSi_2$ matrix for 24 cycles. (b) $MoSi_2$-$30Si_3N_4$ matrix for 200 cycles.

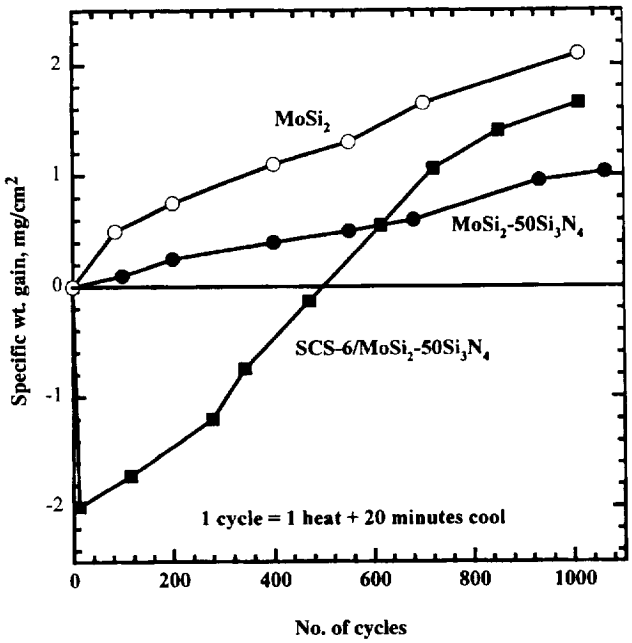

Figure 6.—Specific weight gain versus number of cycles plot for $MoSi_2$-$50Si_3N_4$ monolithic and SCS-6/$MoSi_2$-$50Si_3N_4$ hybrid composite cyclic oxidized at 1250 °C in air.

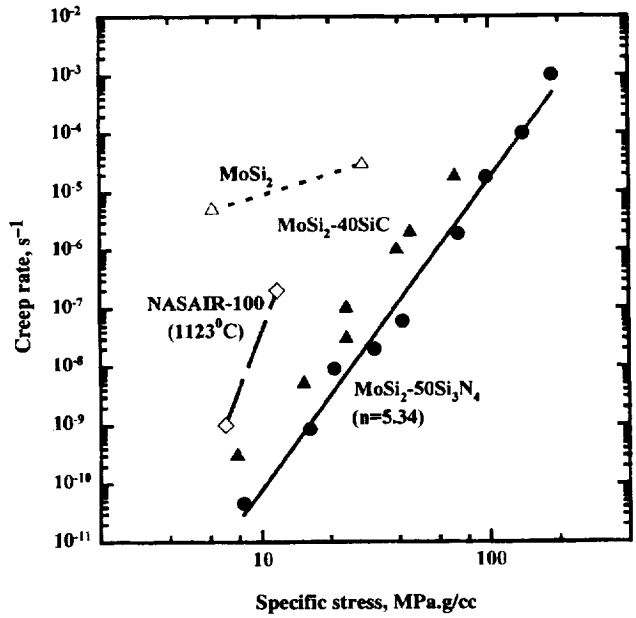

Figure 7.—Second stage creep rate versus specific stress at 1200 °C for $MoSi_2$-$50Si_3N_4$ compared with other materials.

times tougher than the monolithic material. The toughness of the hybrid composite also increased with temperature reaching as high as 65 MPa$\sqrt{m}$, at 1400 °C in argon atmosphere.

Figure 10(a) shows the room temperature tensile stress strain curve for SCS-6/$MoSi_2$-Si_3N_4, indicating composite-like behavior; and three distinct regions, an initial linear region, followed by a non-linear region and a second linear region. The non-linear region is due to the matrix cracking normal to the loading direction. The second linear region is controlled by fiber bundle strength. Individual SCS-6 fibers were tensile tested at room temperature in the as-received, as-etched and etched-from-composite conditions, and produced average strength values of 3.52±0.8, 3.35±0.6, and 3.4±1 GPa, respectively. Thus, neither etching nor consolidation conditions degraded the strength of the fibers, and SEM examination of the fiber surfaces showed no visible differences among the 3 fiber conditions.

Fiber/matrix interfacial properties play an important role in composite mechanical behavior. In the case of this composite system, the carbon layer on SCS-6 provides an appropriate level of bonding that produces adequate strengthening and toughening. The carbon can

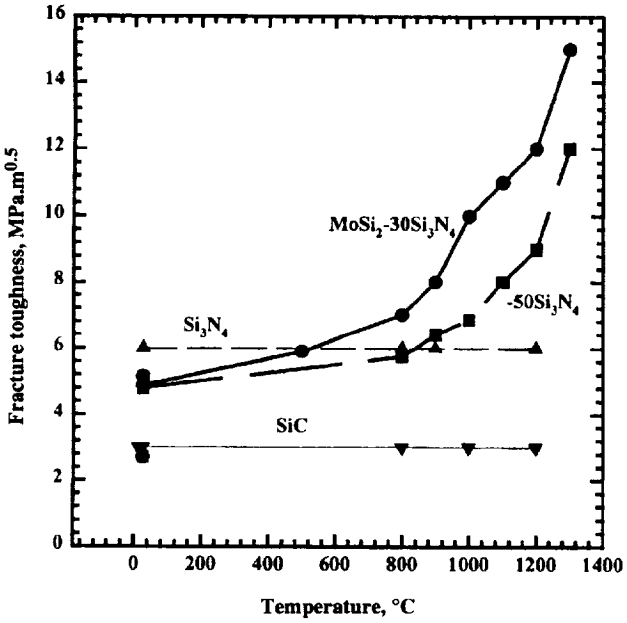

Figure 8.—Temperature dependence of fracture toughness of $MoSi_2$-50Si_3N_4 compared with ceramic matrices.

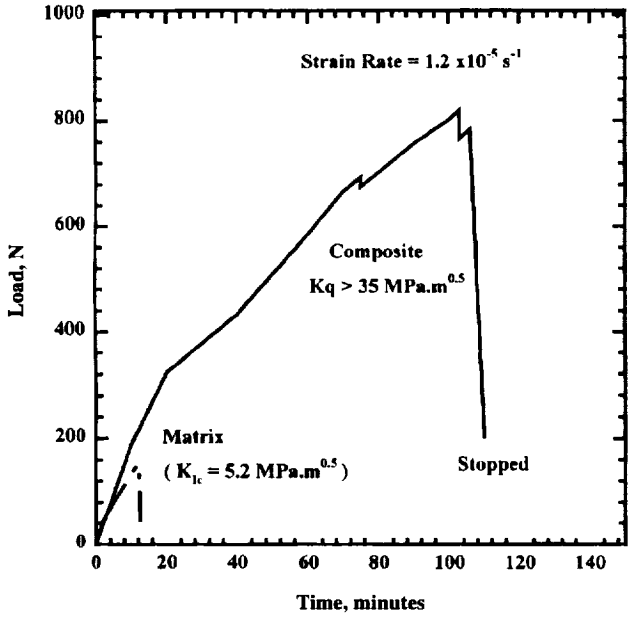

Figure 9.—Load-displacement curves from chevron notched 4 point bend tested SCS-6/$MoSi_2$-50Si_3N_4 and $MoSi_2$-50Si_3N_4 specimen at room temperature.

react with $MoSi_2$ to form SiC and Mo_5Si_3, although the carbon layer is still retained and the reaction zone thickness is not very large at typical HIP temperatures. The fiber matrix interfacial shear strengths determined from a fiber push out test (24) using thin polished sections produced values near 50 MPa, indicating a week bond, between the matrix and the fiber. The interfacial sheer strength for SCS-6/RBSN is about 30 Mpa (24).

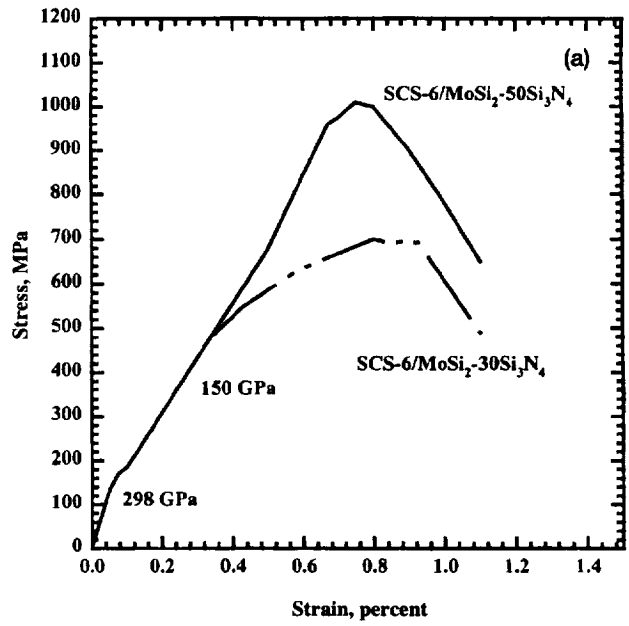

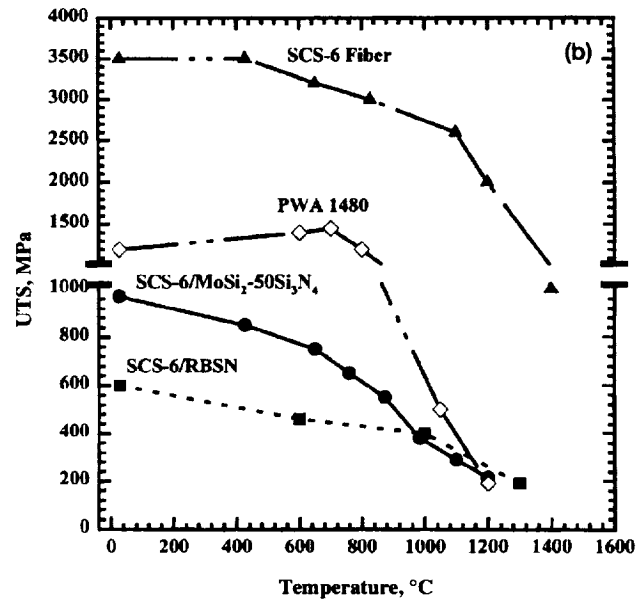

Figure 10.—Mechanical properties of SCS-6/$MoSi_2$-50Si_3N_4 hybrid composites. (a) Room temperature tensile stress-strain curves. (b) Temperature dependence of ultimate tensile strength of SCS-6/$MoSi_2$-50Si_3N_4-base composites compared with other materials.

The ultimate tensile strength increased with an increase in matrix Si_3N_4 content from 30 to 50 vol % which may mean that there is a matrix contribution to the tensile behavior, even after cracking has initiated. Alternatively, a different, higher strength lot of fibers could be responsible for this result. It was also found that the room temperature ultimate tensile strength and strain to fracture were reduced by only 20 percent in a specimen with exposed fibers that was pre-oxidized at 1200 °C for 200 hours. High temperature tensile tests were performed in air at temperatures up to 1400 °C. Stress-strain curves for tests at and above 900 °C did not show evidence of matrix cracking. This can be attributed to the plastic nature of $MoSi_2$

at these temperatures. This is believed to be an advantage over CMC's which exhibit matrix cracking at all temperatures. Figure 10(b) shows the temperature dependence of ultimate tensile strength, along with the data from competitive materials, namely single crystal PWA1480 (25), and SCS-6/reaction bonded silicon nitride(RBSN) (26). PWA 1480 exhibits higher tensile strength than both $MoSi_2$-base and RBSN-base composites between room temperature and 1000 °C; however, PWA 1480 is almost three times denser than both composites, and hence is at a disadvantage on a specific strength basis. Although not included in Fig.10(b) because of different fiber and architecture, typical 2D woven SiC-SiC composites (27) exhibit much lower strengths (~200 MPa) between room temperature and 1200 °C. However, SiC-SiC composites retain their strengths beyond 1200 °C. Figure10(b) also shows the tensile strength data for the SCS-6 fibers, reemphasizing the fiber-dominated behavior of the composites. The $MoSi_2$-base composites also exhibited elastic modulus values of ~290/200 GPa between RT and 1200 °C which were substantially higher than the comparable CMC at all temperatures. Unlike most CMC's which have as much as 20 percent porosity, these $MoSi_2$-base composites are fully dense and hence exhibit higher modulus.

Several tensile creep tests were carried out on SCS-6 (0)/$MoSi_2$-$50Si_3N_4$ composite specimens between 1000 and 1200 °C in vacuum. Unfortunately, it was not possible to get the rupture lives from these specimens due to accidental power failures. Nonetheless, test durations of ~1000 hours were achieved and some idea of long term durability was obtained. Specimens tested at these temperatures exhibited a short primary creep stage and an extended secondary stage. The minimum creep rates ranged from of 1.0×10^{-9} to 2.0×10^{-9} sec^{-1} at 70 MPa between 1100 and 1200 °C.

Impact Properties

Aircraft engine components require sufficient toughness to resist manufacturing defects, assembly damage, stress concentrations at notches, and foreign and domestic object damage (28). Consultation with engine company designers indicated a strong desire for not only fracture toughness but more importantly, impact resistance to be measured before they would seriously consider these types of composites. The Charpy V-notch (CVN) test was chosen to assess impact resistance based on the engine designer's desire to use a relative ranking against more familiar materials, rather than a formal design requirement.

CVN impact tests were conducted on full size specimens of $MoSi_2$-$50Si_3N_4$ matrix and SCS-6 (0) and (0/90) oriented /$MoSi_2$-$50Si_3N_4$ hybrid composites between room temperature and 1400 °C in air. Figure 11(a) shows the force time curves obtained from the instrumented impact tests at room temperature for monolithic $MoSi_2$-$50Si_3N_4$, SCS-6 (0) and (0/90) /$MoSi_2$-$50Si_3N_4$ composites. The maximum value of force represents the elastic energy required for crack initiation. The hybrid composite in (0) orientation exhibited the highest peak force values, followed by the cross-plied and finally the monolithic material. At 1400 °C, the peak force values for all three materials were higher than their corresponding values at room temperature. The hybrid composite exhibited a gradual, stepwise decrease in load after the peak force was achieved. This indicates substantial energy absorption during crack propagation, and was especially pronounced in the (0) orientation.

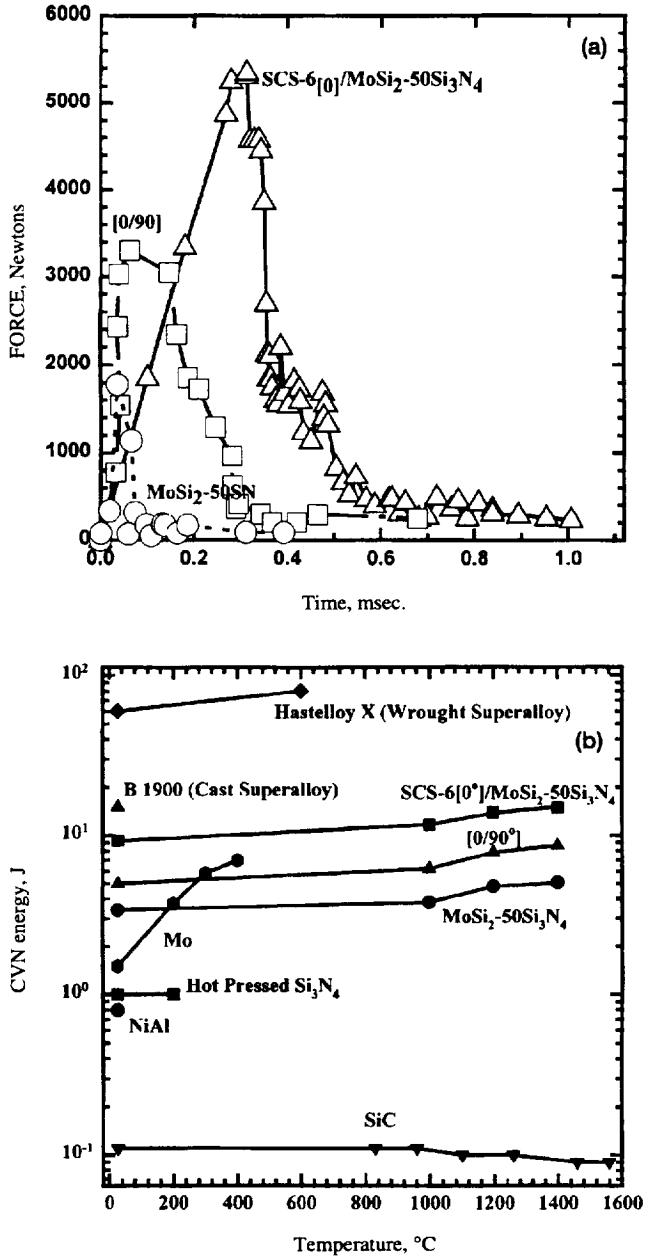

Figure 11.—Impact properties of $MoSi_2$-$50Si_3N_4$ monolithic and SCS-6/$MoSi_2$-$50Si_3N_4$ hybrid composites. (a) Force-time curves obtained from charpy impact tests. (b) CVN energy versus temperature for $MoSi_2$-base composites compared with other materials.

Figure 11(b) shows the temperature dependence of CVN energy for $MoSi_2$-base materials compared with other potential materials such as superalloys, and ceramics. The CVN energy for both the monolithic $MoSi_2$-$50Si_3N_4$ and the hybrid composites increased with increase in temperature. The fiber reinforcement in (0) orientation increased the impact resistance by five times and in (0/90) orientation nearly two times. The CVN energy of SCS-6/$MoSi_2$-$50Si_3N_4$ was comparable to the cast superalloy B-1900 but substantially lower than the wrought superalloy Hastelloy X. The CVN energy of $MoSi_2$-$50Si_3N_4$ monolithic was comparable to Mo alloys and was far superior to NiAl (30), and monolithic Si_3N_4, and SiC. Unlike $MoSi_2$-

$50Si_3N_4$ which shows increased CVN energy with temperature, SiC shows a slight decrease of CVN energy with temperature. This is probably due to the degradation caused by densification aids used with SiC (29). SEM examination of impact tested SCS-6/ $MoSi_2$-$50Si_3N_4$ showed substantial fiber pullout in (0) orientation and limited fiber pullout in (0/90) oriented specimens at all temperatures. Additionally, the SEM image (Fig. 12(a)) showed substantial matrix cracking in the room temperature tested specimens, but only limited cracking at 1400 °C (Fig. 12(b)). This again implies that $MoSi_2$ can behave in a ductile manner at higher temperatures.

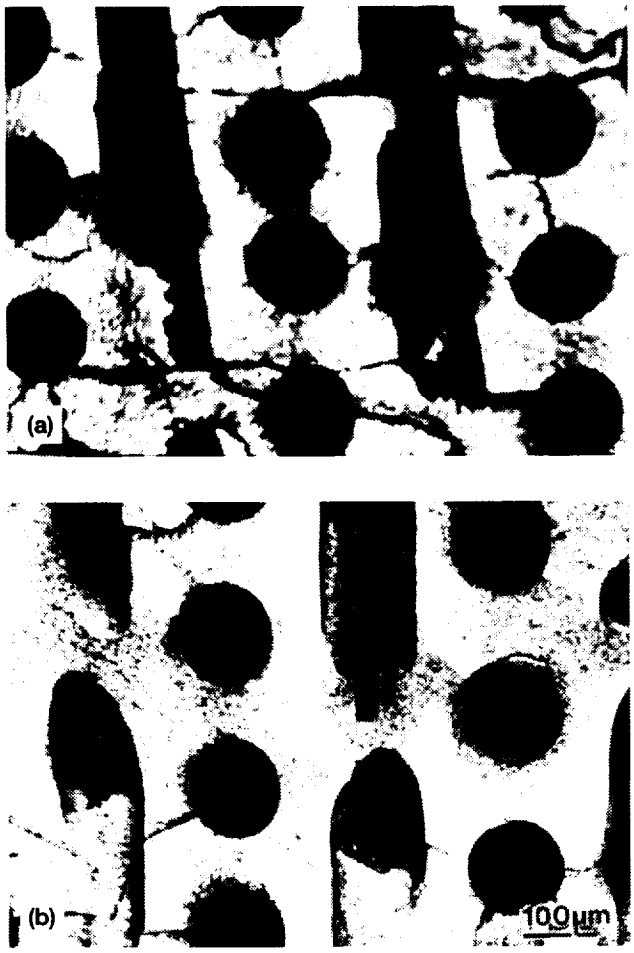

Figure 12.—SEM-BS images of impact tested SCS-6 [0/90]/$MoSi_2$-$50Si_3N_4$ hybrid composites at (a) room temperature and (b) 1400 °C.

Technological Needs: Complex Shapes and Low Cost Processing

Most of the attractive strength and toughness values reported so far were achieved with composites reinforced with SCS-6 fibers made by Textron, Inc. This large diameter (145 μm) fiber was designed primarily for Ti-based composites. This fiber does not have adequate creep strength at the highest temperatures envisioned for $MoSi_2$ and is too large to be bent around the sharp radii needed to make complex shapes. However, it is easy to infiltrate matrix powders between these fibers, thus enabling composites to be fabricated routinely. This ease in fabrication was meant to be exploited by further characterization of key properties such as creep resistance, transverse properties, and performance of the composite in an engine test bed. However, finer diameter fibers are preferred on a cost, shape making, creep resistance, and toughness basis. Hi-Nicalon is the best currently available fiber, although Dow Corning's Sylramic® fiber (developed for the High Speed Civil Transport program), is also appropriate for this $MoSi_2$-Si_3N_4 matrix. A transition in effort to Hi-Nicalon fibers was therefore investigated, first using tow fibers, (i.e., strings of approximately 500 individual filaments that are spread out, wound on a drum and then infiltrated with matrix powder) and ultimately woven cloth (i.e., the tows are woven into two or three dimensional architectures before matrix infiltration).

In earlier studies, the powder cloth technique was used to produce SiC continuous fiber reinforced $MoSi_2$-base composites. The powder cloth process is labor intensive and cannot always produce a uniform fiber distribution. Melt infiltration and chemical vapor infiltration are popular methods for processing of CMC's because of the potential for shape making and lower cost, but are limited to thickness on the order of 5 mm, because segregation and porosity problems are aggravated in thick specimens. Tape casting was therefore adopted as a powder metallurgy method for composite fabrication. Initially, several casting trials of $MoSi_2$-Si_3N_4 were carried out to optimize various parameters such as particle size, type and amount of binder and solvent, flow behavior of the slurry, and binder burn-out cycle. A 56 ply composite of SCS-6/$MoSi_2$-Si_3N_4 was successfully fabricated by tape casting followed by the standard hot press plus HIP consolidation. Composites with small diameter fibers such as SCS-9 (75 μm) and coated Hi-Nicalon (18 to 20 μm) were also successfully fabricated. Figure 13 illustrates the range in fiber diameters in this study. Note also the improvement in fiber spacing control between Fig. 13(a) and Fig. 13(b), achieved by switching from powder cloth to tape casting. Fig. 14 displays efficient spreading of the fiber tows and infiltration of $MoSi_2$-Si_3N_4 powder particles. Although there is still some heterogeneity in the

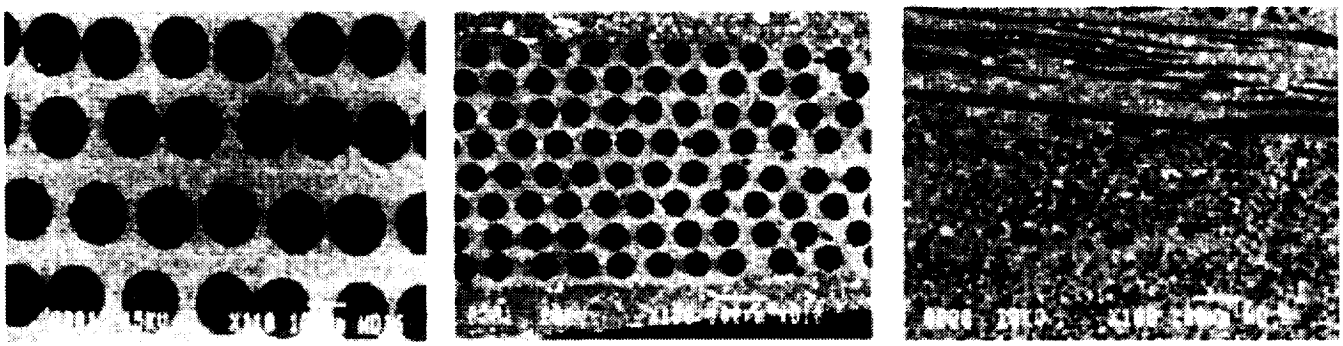

Figure 13.—SEM micrographs of SiC/$MoSi_2$-Si_3-N_4 showing wide range of fiber diameters.

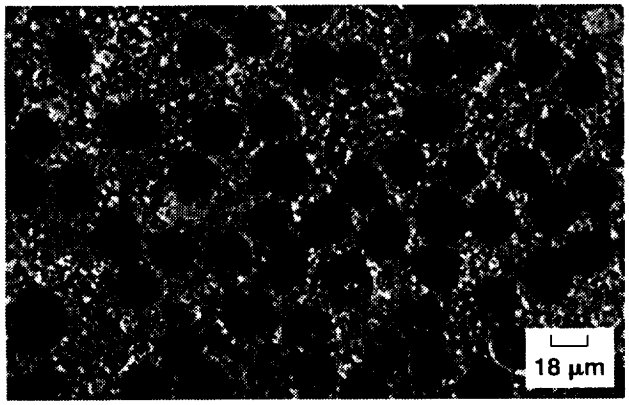

Figure 14.—SEM-SE image of BN/SiC coated Hi-Nicalon/$MoSi_2$-Si_3N_4 hybrid composite showing good fiber spreading and matrix infiltration.

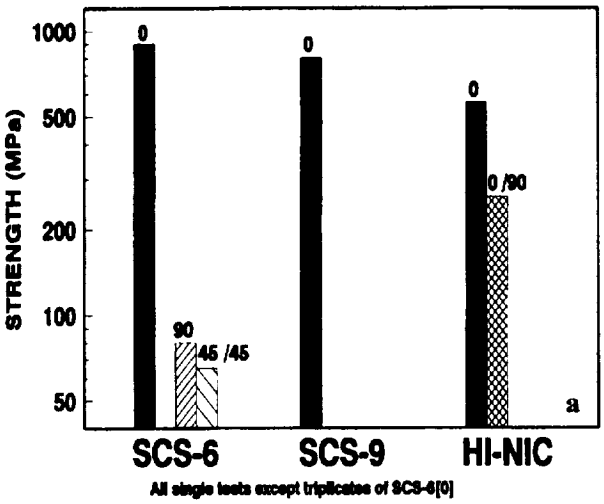

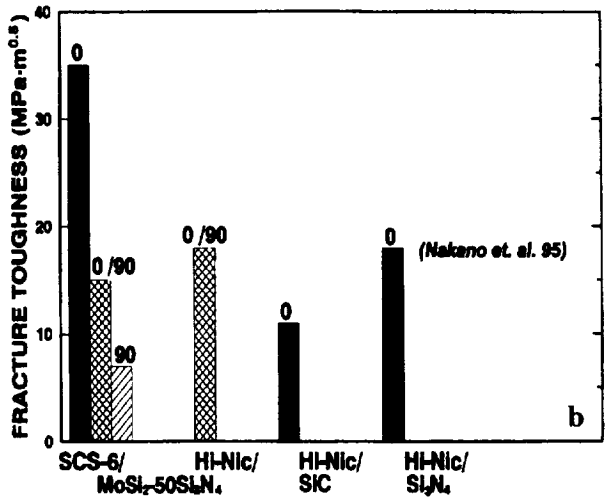

Figure 15.—Influence of fiber diameter and orientation on room-temperature (a) tensile strength and (b) fracture toughness of $MoSi_2$-base hybrid composites.

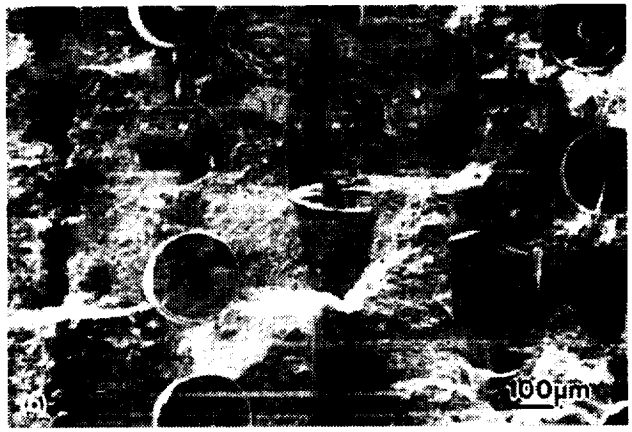

Figure 16.—SEM-SE images of fracture toughness tested (a) BN/SiC coated Hi/Nicalon [0/90]/ (b) SCS-6 [0/90]/ $MoSi_2$-$50Si_3N_4$ hybrid composites.

fiber distribution, this microstructure is among the best we have seen on any other study using fine diameter fibers.

Interfacial coatings play a very important role in fiber reinforced composites, and the Hi-Nicalon tow fibers must be coated before compositing. Interfacial coatings that have proven successful in CMC's have been adopted for use with $MoSi_2$. To date, only carbon or BN have been able to provide the level of interfacial bonding required for toughening, but they both exhibit poor environmental resistance. Therefore, a protective coating of SiC or Si_3N_4 is required as a second layer on top of the debonding layer. Unfortunately, the state of coating technology for fine diameter tows has still not matured to the state where smooth, crack free and uniformly thick coatings can be produced. This immaturity is also reflected in the high cost and limited facilities nationally available for coating. Therefore, only limited mechanical properties have been generated with these fibers.

The influence of fiber diameter and architecture on mechanical properties was investigated by conducting room temperature tensile and fracture toughness tests on specimens of SCS-6, SCS-9 and BN/SiC coated Hi-Nicalon/$MoSi_2$-$50Si_3N_4$ hybrid composites. Testing in the (0) direction (longitudinal) produced the highest strength, (700 to 1000 MPa strength and 1.2 percent total strain) to failure.

Testing in the (90) direction produced the lowest ultimate tensile strength of only 72 MPa and 0.04 % strain to failure for SCS-6 reinforced composite. This is not an unexpected result since the fibers cannot bridge matrix cracks in the transverse direction, and cross-plied laminates or woven 2D or 3D architectures are required to achieve more isotropic properties. For example, the Hi-Nicalon reinforced composite exhibited high strength and strain to failure in the 0/90 architecture, about 60 % of the unidirectional value, Fig. 15(a). Figure 15(b) shows that the Hi-Nicalon/$MoSi_2$-Si_3N_4 in (0/90) direction exhibited higher fracture toughness than the CMC's Hi-Nicalon/SiC and Hi-Nicalon/Si_3N_4, even though they were tested in the more favorable (0) direction (31). The CMC's were processed at much higher temperatures, 1600 to 1800 °C, causing more fiber degradation than Hi-Nicalon/$MoSi_2$-Si_3N_4 and therefore exhibited lower toughness. The SEM micrograph of the fracture toughness tested Hi-Nicalon reinforced composite (Fig. 16(a)) showed more fiber pullout than the SCS-6 fiber reinforced composite (Fig. 16(b)).

Conclusions

A wide spectrum of mechanical and environmental properties have been measured in order to establish feasibility of an $MoSi_2$-base composite with Si_3N_4 particulate and SiC fibers. The high impact resistance of the composite is of particular note, as it was a key property of interest for engine applications. Processing issues have also been addressed in order to lower cost and improve shape making capability. These results indicate that this composite system remains competitive with other ceramics as a potential replacement for superalloys.

Acknowledgments

The authors would like to acknowledge financial support from the Office of the Naval Research, (A.K. Vasudevan) and Pratt & Whitney Aircraft, West Palm Beach, FL (W. Pospisil and R. Hecht), and technical assistance from P. Bartolotta, M. Verrilli, D. Hull and A. Garg.

References

(1) J.R. Stephens, Aviation Week and Space Technology, August 1992.

(2) J. Doychak, Journal of Metals, June (1992), pp. 46–51.

(3) A.K. Vasudevan and J.J. Petrovic, High Temperature Silicides, ed. by A.K. Vasudevan and J.J. Petrovic, North Holland, NY, 1992, pp. 1–17.

(4) J.J. Petrovic and R.E. Honnell, Cerm. Eng. Soc. Proc., 11 (1990) pp. 734–744.

(5) D. J. Shah and D.L. Anton, U.S. Airport Report WRDC-TR-90-4122, Feb. 1991.

(6) S. Bose, High Temperature Silicides, ed., A.K. Vasudevan and J.J. Petrovic, North Holland, NY, 1992, pp. 217–225.

(7) Robert M. Aikin, Jr., Structural Intermetallics, eds., R. Darolia, J.J. Lewandowski, C.T. Liu, D.B. Miracle, and M.V. Nathal, TMS, Warrendale, PA, 1993, pp. 791–798.

(8) K. Sadananda, C.R. Feng and H. Jones, High Temperature Silicides. Ed., A.K. Vasudevan and J.J. Petrovic, North Holland, NY, 1992, pp. 227–237.

(9) J.J. Petrovic R.E. Honnell and W.S. Gibbs, "Moly Disilicide Alloy Matrix Composites", US Patent, 4970, 179.

(10) E. Fitzer and W. Remmele, 5th Int. Conf. on Composite Materials, ICCM-V, AIME (1985), pp. 515–530.

(11) M.J. Maloney and R.J. Hecht, High Temperature Silicides, ed., A.K. Vasudevan and J.J. Petrovic, North Holland, NY, 1992, pp. 19–31.

(12) P.J. Meschter, Met. Trans., Vol. 23A, 1992.

(13) T.C. Chou and T.G. Nieh, J. Mater. Res. Vol 8, No. 1, 1993, pp. 214–223.

(14) D.A. Berztiss, R.R. Cerachiara, E.A. Gulbransen, F.S. Pettit and G.H. Meier, Materi. Sci. Eng., A155, 1992, pp. 165–181.

(15) A. Muller, G. Wang, R.A. Rapp, High Temperature Silicides, Eds., A.K. Vasudevan, J.J. Petrovic, North Holland, Amsterdam, London, NY, 1992, pp. 199–209.

(16) S.V. Raj, Mat. Sci. Eng., A201, 1995. pp. 229–241.

(17) M.G. Hebsur, Intermetallic Composites III, Ed. by J.A. Graves, R.R. Bowman, and J.J. Lewandowski, MRS Proc., Vol. 350, 1994, Pittsburgh, PA, pp. 177–182.

(18) M.G. Hebsur, "Pest Resistant $MoSi_2$ Materials and Method of Making" U.S. Patent, No. 5, pp. 429, 997, 1995.

(19) J.W. Pickens, NASA TM–102060, 44135, 1989 NASA LeRC, Cleveland, OH.

(20) M.V. Nathal and L.J. Ebert, Metall. Trans., 16 A, 1985 427-439.

(21) I.J. Blum, Eng. Fract. Mech., 1975 pp. 593-604.

(22) A. Ghosh, M.G. Jenkins, M.K. Ferber, J. Peussa and J.A. Salem, Eds., R.C. Bradt et al., Plenum Press, New York, 1992.

(23) A.J. Pyzik and D.R. Beaman J. Am. Ceram. Soc., 76, pp. 2737–2744, 1993.

(24) J.I. Eldridge, R.T. Bhatt and J.D. Kaiser, NASA TM–103739, 1991, NASA Lewis Research Center, Cleveland, OH.

(25) M.G. Hebsur and R.V. Miner, NASA TM–88950, 1987, NASA Lewis Research Center, Cleveland, OH.

(26) R.T. Bhatt., NASA CP–10039, 1989, pp. 57-1-57-13, NASA Lewis Research Center, Cleveland, OH.

(27) J. Halada, "Enhanced SiC/SiC Ceramic Matrix Composites for Long Life Performance in Oxidizing Environments", Du-Pont Lanxide Composites Report, January 1994.

(28) P.K. Wright, Structural Intermetallics, eds. R. Darolia, J.J. Lewandowski, C.T. Liu, D.B. Miracle, and M.V. Nathal, TMS, Warrendale, PA, 1993, pp. 885–893.

(29) R.C. Bradt, NASA CR–165325, 1984, NASA, Washington D.C.

(30) V.C. Nardone, Met., Trans., Vol., 23A, 1992, pp. 563–572.

(31) K.Nakano, K. Sasaki, H. Saka, M. Fujikura, and H. Ichikawa, High Temperature Ceramic-Matrix Composites II, Manufacturing and Materials Development, ed. by A.G. Evans, R.N. Nasalin, 1995, pp. 215–229.

REPORT DOCUMENTATION PAGE

Form Approved
OMB No. 0704-0188

1. AGENCY USE ONLY (*Leave blank*)	2. REPORT DATE	3. REPORT TYPE AND DATES COVERED
	September 1997	Technical Memorandum

4. TITLE AND SUBTITLE

Strong, Tough, and Pest Resistant $MoSi_2$–Base Hybrid Composite for Structural Applications

5. FUNDING NUMBERS

WU–523–22–13

6. AUTHOR(S)

M.G. Hebsur and M.V. Nathal

7. PERFORMING ORGANIZATION NAME(S) AND ADDRESS(ES)

National Aeronautics and Space Administration
Lewis Research Center
Cleveland, Ohio 44135–3191

8. PERFORMING ORGANIZATION REPORT NUMBER

E–10759

9. SPONSORING/MONITORING AGENCY NAME(S) AND ADDRESS(ES)

National Aeronautics and Space Administration
Washington, DC 20546–0001

10. SPONSORING/MONITORING AGENCY REPORT NUMBER

NASA TM–107471

11. SUPPLEMENTARY NOTES

Prepared for the Second International Symposium on Structural Intermetallics sponsored by The Minerals, Metals, and Materials Society, Seven Springs, Pennsylvania, September 21–26, 1997. M.G. Hebsur, NYMA, Inc., 2001 Aerospace Parkway, Brook Park, Ohio 44142 (work funded by NASA Contract NAS3–27186) and M.V. Nathal, NASA Lewis Research Center. Responsible person, M.V. Nathal, organization code 5120, (216) 433–9516.

12a. DISTRIBUTION/AVAILABILITY STATEMENT

Unclassified - Unlimited
Subject Category 27

This publication is available from the NASA Center for AeroSpace Information, (301) 621–0390.

12b. DISTRIBUTION CODE

13. ABSTRACT ***(Maximum 200 words)***

Addition of about 30 to 50 vol % of Si_3N_4 particulate to $MoSi_2$ improved resistance to low temperature accelerated oxidation by forming a Si_2ON_2 protective scale and thereby eliminating catastrophic 'pest failure'. The Si_3N_4 addition also improved the high temperature creep strength by nearly five orders of magnitude, doubled the room temperature toughness and significantly lowered the CTE of the $MoSi_2$ and eliminated matrix cracking in SCS-6 reinforced composites even after thermal cycling. The SCS-6 fiber reinforcement improved the room temperature fracture toughness by seven times and impact resistance by five times. The composite exhibited excellent strength and toughness improvement up to 1400 °C. More recently, tape casting was adopted as the preferred processing of $MoSi_2$-base composites for improved fiber spacing, ability to use small diameter fibers, and for lower cost. Good strength and toughness values were also obtained with fine diameter Hi-Nicalon tow fibers. This hybrid composite remains competitive with ceramic matrix composites as a replacement for Ni-base superalloys in aircraft engine applications.

14. SUBJECT TERMS

Pesting; Si_3N_4 particulate; Tensile strength; Impact resistance; Hi Nicalon, Hybrid composite, $MoSi_2$

15. NUMBER OF PAGES

12

16. PRICE CODE

A03

17. SECURITY CLASSIFICATION OF REPORT	18. SECURITY CLASSIFICATION OF THIS PAGE	19. SECURITY CLASSIFICATION OF ABSTRACT	20. LIMITATION OF ABSTRACT
Unclassified	Unclassified	Unclassified	